

Status of the Mu2e experiment

Stefano Di Falco^{a,*} for the Mu2e collaboration*

^aINFN Pisa,

Largo B. Pontecorvo 3, Pisa, Italy

E-mail: stefano.difalco@pi.infn.it

The Mu2e experiment at Fermilab aims to measure the charged-lepton flavour violating (CLFV) neutrino-less conversion of a negative muon into an electron in the field of a nucleus with an unprecedented single event sensitivity of $3 \cdot 10^{-17}$. This document illustrates the physics motivation and design of the experiment.

In the current schedule Mu2e is expected to start taking data in 2025 with a reduced average beam intensity for about two years (Run 1). After a shut down for the upgrade of Fermilab accelerator complex, data taking will restart at full beam intensity (Run 2). A detailed update of the expected experiment sensitivity for Mu2e Run 1 is presented, together with an estimate of the final Mu2e sensitivity.

*** *The European Physical Society Conference on High Energy Physics (EPS-HEP2021)*, ***

*** *26-30 July 2021* ***

*** *Online conference, jointly organized by Universität Hamburg and the research center DESY* ***

*[Mu2e Collaboration List, 2021](#).

*Speaker

1. Overview of the Mu2e experiment

The Mu2e experiment[1] at Fermilab Muon Campus will search for the charged-lepton flavour violating (CLFV) neutrino-less conversion of a negative muon into an electron (CE) in the field of an nucleus:



The spectrum of the produced electron is nearly monochromatic with a peak energy slightly lower than the muon rest mass (104.97 MeV)¹.

The current best limit on this process comes from Sindrum II experiment that has set an upper limit at 90% CL on the ratio between muon conversions and muon nuclear captures in Gold [2]:

$$R_{\mu e} = \frac{N(\mu \rightarrow e)}{N(\text{nuclear captures})} < 7 \cdot 10^{-13} \text{ (90\% CL)} \quad (2)$$

The goal of Mu2e is to improve this limit by four orders of magnitude or actually observe CLFV directing an intense muon beam on an Aluminum target. This big improvement in sensitivity will allow Mu2e to check many possible extensions of the Standard Model that predict an $R_{\mu e}$ value in the range that can be observed by the experiment[3].

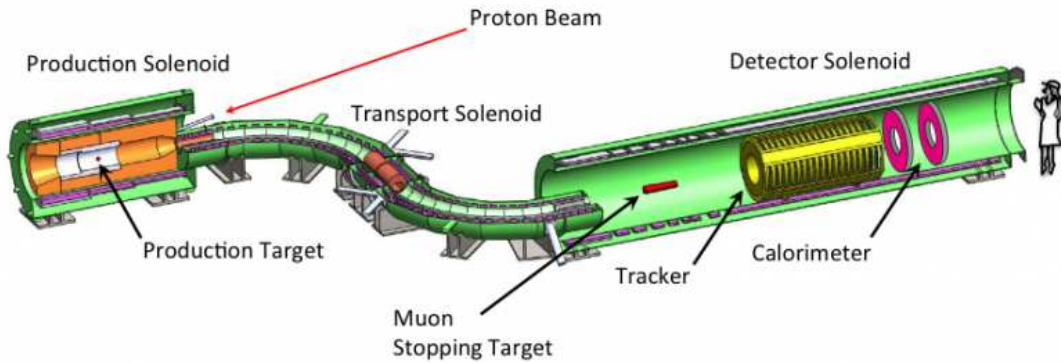


Figure 1: The Mu2e experimental apparatus.

The Mu2e apparatus is shown in Fig.1: an 8 GeV pulsed proton beam is sent to a tungsten target located in the Production Solenoid (PS). The PS produces a graded magnetic field varying from 4.5T to 2.5T, that improves the acceptance of the next magnetic element, the Transport Solenoid (TS) for low momentum particles. The TS, with its particular “S” shape, selects charged particles of the wanted momentum using a graded toroidal field (from 2.5T to 2T) and a set of collimators that can be rotated to choose the sign of the charge. At the entrance and in the middle of TS two absorber windows are used to suppress the antiproton background. The last solenoid, the Detector Solenoid (DS), hosts the Aluminum stopping target, surrounded by two proton absorbers that reduce the radiation in the detectors region, the straw tube tracker and the electromagnetic calorimeter. Also the DS has a graded magnetic field varying from 2T to 1T. The field in the tracker-calorimeter region is uniform (1T) to guarantee the best accuracy in the momentum reconstruction.

¹A small low energy tail is due to nuclear recoils and radiative corrections.

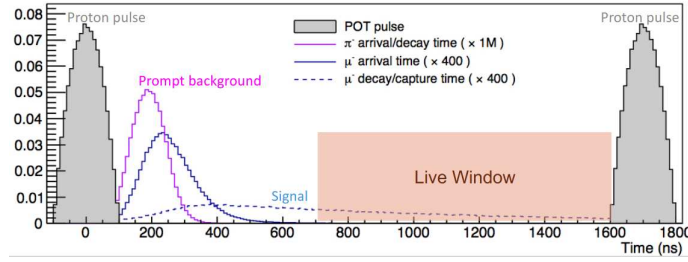


Figure 2: Mu2e pulsed proton beam structure.

The structure of the pulsed proton beam is shown in Fig.2. The time interval between two proton spills is $\sim 1.7 \mu\text{s}$ and well matches the muonic Al lifetime (864 ns). A delayed analysis window starting from ~ 700 ns is used to suppress the prompt background while keeping a good efficiency on the muon conversions. The fraction of protons out of spill, expected to be lower than 10^{-10} , will be monitored by a detector observing the particles scattered from the production target.

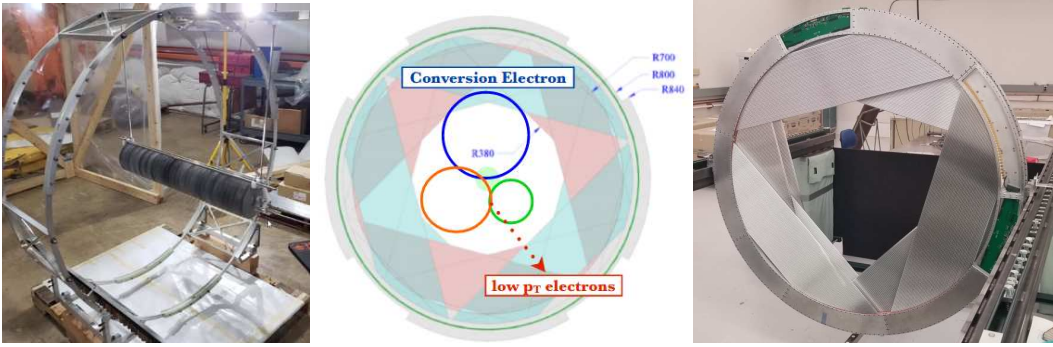


Figure 3: Left: the Aluminum Stopping Target. Center: tracker transverse view. Right: two tracker planes.

The Aluminum Stopping Target (Fig.3) has a segmented structure (37 disks $100 \mu\text{m}$ thick) to minimize the energy loss. A central hole reduces the amount of bremsstrahlung radiation reaching the detectors.

The tracker is made of ~ 21000 straw tubes, with a diameter of 5 mm and a thin wall of $15 \mu\text{m}$ of mylar, filled with a 80%-20% Ar-CO₂ gas mixture. The anode is a $25 \mu\text{m}$ tungsten wire at 1450 V read by ADCs and TDCs at both ends. Straw tubes of variable length are disposed in a double-layer 120° circular segment (panel) covering a radius from 380 mm to 700 mm. Three panels rotated with steps of 120° form a plane. Two planes rotated by 60° form a station. There are 18 stations disposed along the beam axis, for a total tracker length of ~ 3.3 m. The central hole makes the tracker insensitive to particles produced in the stopping target with a momentum lower than $\sim 80 \text{ MeV}/c^2$ and to the remnant beam (Fig.3). The hit coordinate resolutions measured on a panel prototype ($283 \mu\text{m}$ in the transverse direction and 43.4 mm along the wire) are in agreement with Monte Carlo

²In particular the vast majority of the electrons produced by the muon decays in the orbit (DIO) of the Al atom have a momentum lower than 52 MeV/c (Michel's edge) and do not produce hits in the tracker.

expectations. The reconstructed CE momentum distribution obtained by the simulation is nearly gaussian with a FWHM of 0.96 MeV/c and a small low momentum tail mainly due to energy losses.

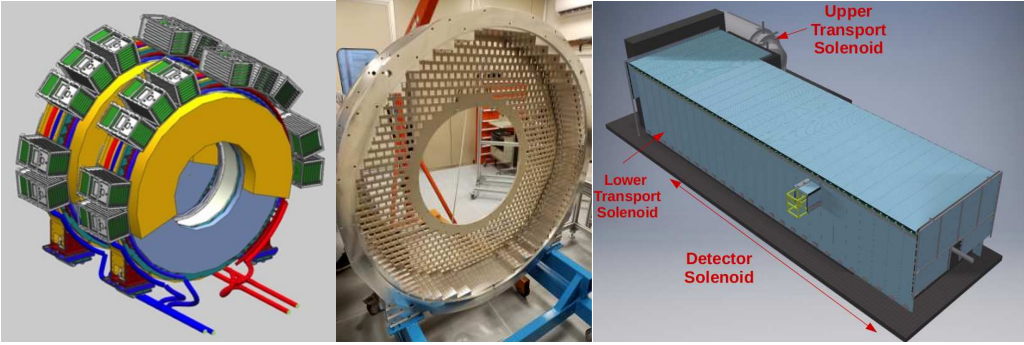


Figure 4: Left: ECAL disks. Center: ECAL disk mechanical structure. Right: CRV layout.

The electromagnetic calorimeter (ECAL) is made of 2 disks of pure CsI crystals. The disks also have an annular shape, with an inner radius of 374 mm and an outer radius of 660 mm. The disks are spaced by 700 mm to allow the second disk to detect the electrons passing through the hole of the first one. Each disk contains 674 crystals of equal dimensions ($34 \times 34 \times 200 \text{ mm}^3$). Each crystal is read by 2 arrays of 6 SiPMs. Preamplifier boards sit just on the back of the SiPMs while the slow control and digital electronics are hosted in crates mounted all around the disks (Fig.4). Test beam results have shown an energy resolution of $\sim 7\%$ and a single sensor time resolution of $\sim 230 \text{ ps}$ on 100 MeV electrons with 50° impact angle[4].

The main goal of the calorimeter is to reject cosmic ray muons that mimick the conversion electron signal. A particle identification ANN classifier using the particle time of flight from the tracker to the ECAL and the ratio between the energy measured by the calorimeter and the momentum measured by the tracker is able to suppress the muons by a factor > 100 while introducing a negligible inefficiency for the electron signal.

About 1 cosmic ray event per day will mimic a 105 MeV/c electron. The main part of this background will be rejected by the Cosmic Ray Veto (CRV) system (Fig. 4): four layers of scintillator counters — read by WLS fibers — surround the DS and the last part of the TS. Each fiber is read at both ends by SiPMs. The CRV is expected to recognize 99.99% of the charged cosmic particles crossing it. This challenging performance will be monitored exploiting a large amount of data acquired with beam off during normal runs.

2. Expected sensitivity

The proton beam is expected to be ready for late 2024. A first run (Run 1), mostly with reduced beam duty cycle, is expected to improve by a factor 10^3 over the current world limit in two years. After the accelerator shutdown for the LBNF facility construction, data taking will restart in 2029 to reach the final goal of a 10^4 improvement in about 3 additional years.

A simulation campaign, using the results of the tests on the first subdetectors prototypes and the updated schedule, has been used to estimate the number of background events expected in Run 1. The analysis has included track quality selection, particle identification and cosmic rejection.

The dominant background is due to cosmic rays. About 75% of them are muons that enter from the TS eluding CRV and interact in TS material producing electrons.

The second largest background is given by muon Decays In Orbit (DIO) in the stopping target³. The spectrum of the electrons produced by these decays extends up to the conversion electron energy with a $(E_{CE} - E)^5$ law when approaching the end point. Fig. 5 shows the DIO and CE spectra after that the analysis cuts have been applied.

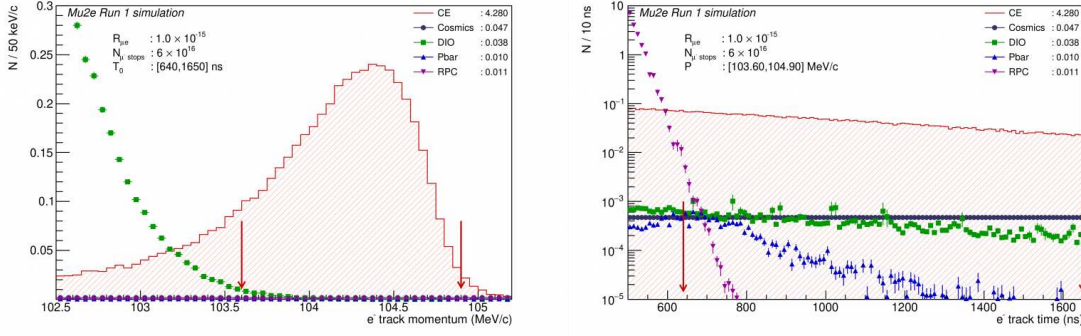


Figure 5: Run 1 expected momentum (left) and time (right) distributions for the CE signal (assuming $R_{\mu e} = 10^{-15}$) and the main backgrounds.

Other relevant backgrounds are due to antiprotons and Radiative Pion Captures (RPCs). The antiproton background can only be reduced with the use of absorbers placed along the beam line. The electrons produced by the internal or external conversions of the photons from RPC have a time distribution much different from the one of the muon conversions so they can be efficiently rejected by a time cut (Fig. 5). The time distribution for cosmic background is flat while the one for CEs and DIOs is determined by the muonic Aluminum lifetime.

The momentum and time selection windows have been optimized to achieve the best “ 5σ discovery sensitivity”, that is the minimal number of signal events corresponding to a 5σ excess⁴ with respect to the background only hypothesis. The expected number of background events corresponding to the optimized cuts ($103.6 < p < 104.9$ MeV/c and $640 < t < 1650$ ns) is reported in Table 1. The sensitivity optimization has been done varying the background expectations within their errors.

Given the very low background level, a 5σ discovery in Run 1 will require Mu2e to observe just 5 events of muon conversion, corresponding to:

$$R_{\mu e}^{5\sigma} = 1.1 \cdot 10^{-15} \quad (3)$$

If no events will be observed in Run 1 Mu2e will improve the 90% CL limit⁵ to:

$$R_{\mu e} < 5.9 \cdot 10^{-16} \text{ (90\% CL) [Mu2e Run 1]} \quad (4)$$

that is more than x1000 better than current world limit. In Run 2 this limit could be lowered by an additional factor 10 in about 3 years of running.

³About 39% of the muons in the muonic Aluminum decay in orbit; the rest is captured by the nucleus.

⁴This corresponds to a one-sided gaussian probability of $p = 2.86 \cdot 10^{-7}$.

⁵Determined using the Feldman Cousins approach[5].

Channel	Mu2e Run 1 Background Expectation
Cosmics	0.048 ± 0.010 (stat) ± 0.010 (syst)
DIO	0.038 ± 0.002 (stat) $^{+0.026}_{-0.016}$ (syst)
Antiprotons	0.010 ± 0.003 (stat) $^{+0.010}_{-0.004}$ (syst)
RPC	0.011 ± 0.002 (stat) $^{+0.001}_{-0.002}$ (syst)
Total	0.107 ± 0.032 (stat \oplus syst)

Table 1: Run 1 expected backgrounds.

3. Summary

Mu2e construction is under way. Prototypes test and simulation confirm the design detector performances. A first run in 2025-2026 is expected to improve the SINDRUM II limit by a factor 10^3 . A second run, starting in 2029, will allow to improve by 10^4 this limit and to test several possible extensions of the Standard Model predicting CLFV.

4. Acknowledgments

We are grateful for the vital contributions of the Fermilab staff and the technical staff of the participating institutions. This work was supported by the US Department of Energy; the Istituto Nazionale di Fisica Nucleare, Italy; the Science and Technology Facilities Council, UK; the Ministry of Education and Science, Russian Federation; the National Science Foundation, USA; the Thousand Talents Plan, China; the Helmholtz Association, Germany; and the EU Horizon 2020 Research and Innovation Program under the Marie Skłodowska-Curie Grant Agreement No. 690835, 734303, 822185, 858199. This document was prepared by members of the Mu2e Collaboration using the resources of the Fermi National Accelerator Laboratory (Fermilab), a U.S. Department of Energy, Office of Science, HEP User Facility. Fermilab is managed by Fermi Research Alliance, LLC (FRA), acting under Contract No. DE-AC02-07CH11359.

References

- [1] L. Bartoszek et al., *Mu2e Technical Design Report, Fermilab-TM-2594, Fermilab-DESIGN-2014-1, arXiv:1501.05241* (2014).
- [2] Wilhelm H. Bertl et al., *A Search for muon to electron conversion in muonic gold, Eur. Phys. J. C***47** (2006) 337.
- [3] W. Altmannshofer et al., *Anatomy and Phenomenology of FCNC and CPV Effects in SUSY Theories, arXiv:0909.1333v2* (2010).
- [4] N. Atanov et al., *Electron beam test of the large area Mu2e calorimeter prototype*, in proceedings of *18th International Conference on Calorimetry in Particle Physics (CALOR 2018)*.
- [5] G.J. Feldman and R. D. Cousins, *Unified approach to the classical statistical analysis of small signals, Phys. Rev. D***57** (1998) 3873.